

Microscopic nature of correlations in multiorbital $A\text{Fe}_2\text{As}_2$ ($A = \text{K}, \text{Rb}, \text{Cs}$): Hund's coupling versus Coulomb repulsion

Steffen Backes,^{*} Harald O. Jeschke, and Roser Valentí*Institut für Theoretische Physik, Goethe-Universität Frankfurt, Max-von-Laue-Str. 1, 60438 Frankfurt am Main, Germany*

(Received 5 August 2015; revised manuscript received 12 October 2015; published 16 November 2015)

We investigate via LDA+DMFT (local density approximation combined with dynamical mean field theory) the manifestation of correlation effects in a wide range of binding energies in the hole-doped family of Fe pnictides $A\text{Fe}_2\text{As}_2$ ($A = \text{K}, \text{Rb}, \text{Cs}$) as well as the fictitious FrFe_2As_2 and a -axis stretched CsFe_2As_2 . This choice of systems allows for a systematic analysis of the interplay of Hund's coupling J_H and on-site Coulomb repulsion U in multiorbital Fe pnictides under *negative* pressure. With increasing ionic size of the alkali metal, we observe a nontrivial change in the iron $3d$ hoppings, an increase of orbitally-selective correlations, and the presence of incoherent weight at high binding energies that do not show the typical lower Hubbard-band behavior but rather characteristic features of a Hund's metal. This is especially prominent in ab -stretched CsFe_2As_2 . We also find that the coherent/incoherent electronic behavior of the systems is, apart from temperature, strongly dependent on J_H , and we provide estimates of the coherence scale T^* . We discuss these results in the framework of reported experimental observations.

DOI: [10.1103/PhysRevB.92.195128](https://doi.org/10.1103/PhysRevB.92.195128)

PACS number(s): 71.15.Mb, 71.27.+a, 74.25.Jb, 74.70.Xa

I. INTRODUCTION

The nature and degree of correlations in Fe-based superconductors has been a subject of intensive discussions since the discovery of the first high- T_c iron pnictide superconductor in 2008 [1]. A significant amount of work has concentrated on the description of experimentally observed effects of correlation like large effective masses or possible non-Fermi liquid behavior [2–8]. Due to the multiorbital nature of Fe-based superconductors, the Hund's coupling J_H has been shown to play a key role in determining the behavior of these systems [2,5–11]. However, there is an ongoing debate regarding the role of J_H versus the on-site Coulomb repulsion U and the interpretation of the correlated nature of Fe pnictides and Fe chalcogenides [2,4,5,11–15]. An important feature observed in many of these studies is that, depending on the electronic filling, the Hund's coupling J_H on the one hand renders a moderately correlated system even more correlated and pushes it into a bad metal regime, while on the other hand it can also reestablish a metallic behavior, albeit orbitally selective, in a strongly correlated system [11,15]. The main question for the Fe-based superconductors narrows down to which regime of parameters do they belong to and how do correlations manifest themselves in a wide range of binding energies as a function of doping and/or pressure?

Of special interest are the hole-doped $A\text{Fe}_2\text{As}_2$ ($A = \text{K}, \text{Rb}, \text{Cs}$) end members of the 122 iron pnictide series. Compared to the parent compound BaFe_2As_2 , the substitution of Ba by K accounts for a doping of one hole per formula unit, and it is accompanied by a complete suppression of any structural or magnetic phase transition [16,17] and by the appearance of superconductivity at low temperatures. This behavior is common [18–22] to all hole-doped end members $A\text{Fe}_2\text{As}_2$, and they all seem to have a nodal gap structure [18,23], which is different from the nodeless gap structure found in the parent BaFe_2As_2 system [24–26]. Further, experimentally $\text{Ba}_{1-x}\text{K}_x\text{Fe}_2\text{As}_2$ is

thought to undergo a coherence-incoherence transition [27–29] as a function of temperature that has been interpreted in terms of a strong increase in correlations [30–32]. Measurements of the Sommerfeld coefficient suggest that the hole-doped end systems are among the strongest correlated 122 iron-pnictide superconductors [20,27], which is also corroborated by theoretical investigations on KFe_2As_2 [4,12,27,33,34]. The measured Sommerfeld coefficient increases from BaFe_2As_2 to KFe_2As_2 by more than an order of magnitude [27,35,36] and increases further as K is substituted by Rb and Cs [19,37]. In view of these observations, the hole-doped end members $A\text{Fe}_2\text{As}_2$ provide an ideal background for investigating correlation effects as a function of *negative* pressure.

In the present paper we analyze via a combination of density functional theory (DFT) in the local density approximation (LDA) with dynamical mean field theory (LDA+DMFT) the electronic structure of the series $A\text{Fe}_2\text{As}_2$ ($A = \text{K}, \text{Rb}, \text{Cs}$) as well as the fictitious FrFe_2As_2 and a -axis stretched CsFe_2As_2 in an extended range of binding energies. The combination of density functional theory with many body methods such as dynamical mean field theory has proven to be a very helpful tool to investigate electronic correlation effects [38–41]. While a compression of the unit cell usually decreases correlation effects in the 122 iron pnictides [42–44] similarly, the opposite is to be expected when lattice parameters are expanded since the larger interatomic distances should reduce the hybridization of neighboring atomic orbitals and lead to stronger localization of the electronic states. We show in this study that these considerations are correct only at first sight; actually, the strong correlation effects in these systems are mostly governed by a subtle interplay of J_H and U .

II. RESULTS AND DISCUSSION

We performed DFT(LDA) and LDA+DMFT calculations on experimental structures of KFe_2As_2 , RbFe_2As_2 , and CsFe_2As_2 [45] in tetragonal symmetry. Additionally, we prepared a fictitious structure for FrFe_2As_2 with lattice parameters

*backes@itp.uni-frankfurt.de

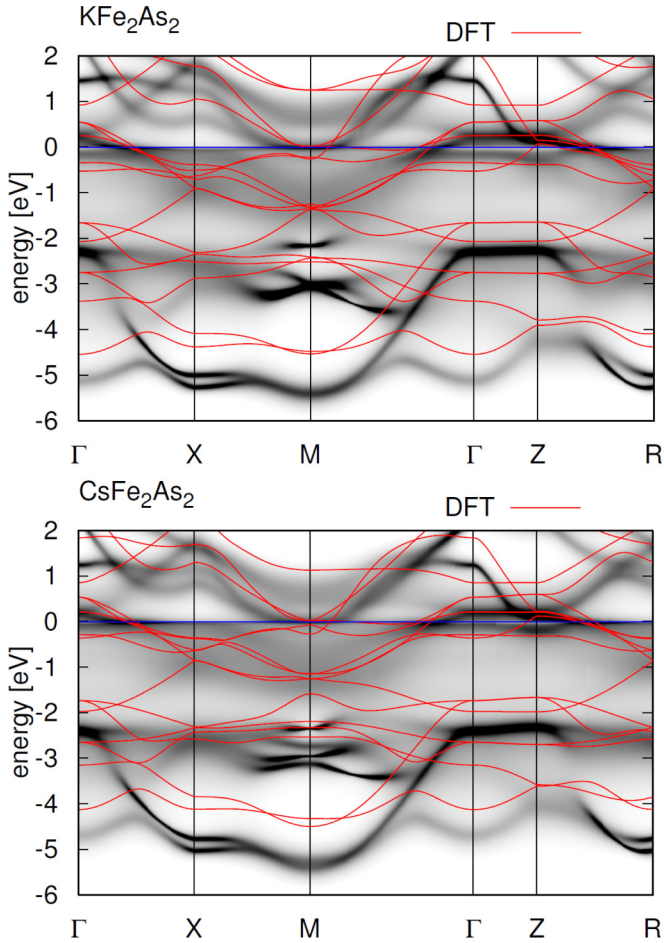


FIG. 1. (Color online) Momentum-resolved spectral function of KFe_2As_2 (top) and CsFe_2As_2 (bottom). Strong correlations in these materials introduce renormalization effects as well as broadening in the spectral function due to finite quasiparticle lifetimes compared to DFT(LDA). We observe a notable broadening and suppression of spectral features especially in the energy range $[-2.0, -0.5]$ eV.

and As height obtained by extrapolating the experimental parameters for $A\text{Fe}_2\text{As}_2$ ($A = \text{K}, \text{Rb}, \text{Cs}$) (see Appendix A). Furthermore, we considered an a -axis stretched CsFe_2As_2 structure by slightly expanding the lattice of CsFe_2As_2 in the ab plane to mimic an experimental biaxial stretching of the crystal. This may be achieved experimentally by epitaxial growth of CsFe_2As_2 on a substrate with slightly larger lattice parameter. The structural trends of this series are an expansion along a and c and a decrease of the As height. A detailed explanation of the structures and computational methods is given in Appendix A.

A. Momentum-resolved spectral function $A(\mathbf{k}, \omega)$

In Fig. 1 we show the momentum-resolved spectral function for KFe_2As_2 and CsFe_2As_2 as obtained within LDA+DMFT (gray density plot) at a temperature $T = 145$ K and compare it to the DFT band structure (red). We estimate for both systems Fe $3d$ effective masses m^*/m_{LDA} between 2.2 and 4.1 (depending on the orbital) which lead to a renormalization of the DFT(LDA) band energies and overall reduction of

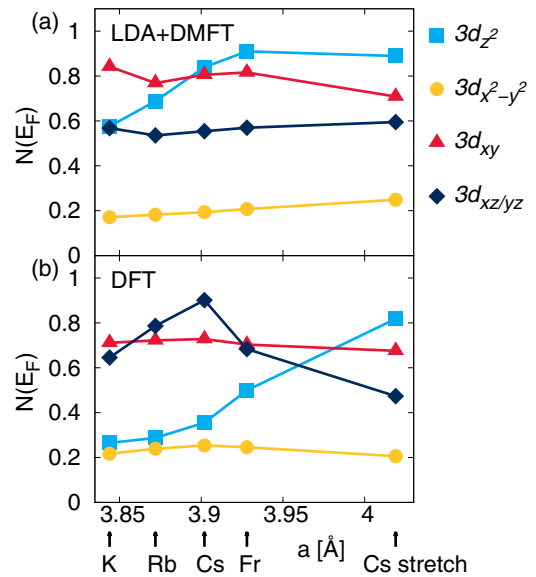


FIG. 2. (Color online) The density of states of the Fe $3d$ orbitals at the Fermi level as obtained from (a) LDA+DMFT and as comparison with (b) DFT. The electronic correlations induce a marked deviation from the DFT results: The contribution of the Fe $3d_{z^2}$ orbital is strongly enhanced, while a more pronounced decrease of the Fe $3d_{xy}$ orbital is found towards the end system of stretched CsFe_2As_2 . Also, the trend in the Fe $3d_{xz/yz}$ orbital in DFT is completely evened out in LDA+DMFT.

bandwidth. The average effective mass increases slightly from 2.89 to 2.95, which indicates an increase in correlation along the $A\text{Fe}_2\text{As}_2$ series due to enhanced localization of electrons on Fe. Already at the Fermi level we obtain diffuse structures corresponding to incoherent quasiparticle excitations with finite lifetimes. At energies below -0.5 eV all coherent features are basically washed out due to correlation. This effect is present in all systems in the series $\text{KFe}_2\text{As}_2 \rightarrow \text{CsFe}_2\text{As}_2$, where we observe an energy range of strong broadening and depletion of spectral weight compared to the DFT band structure between $[-2.0, -0.5]$ eV. At energies below -2 eV coherent features become visible again, which correspond to the As $4p$ states that partially hybridize with Fe $3d$ states. Even though the self-energy in DMFT has no momentum dependence, an effective momentum dependence is present in the results due to the momentum dependent orbital character of the original DFT bands. This leads to k -dependent broadening effects in LDA+DMFT.

B. Density of states at the Fermi level and orbital-resolved electronic filling

We first analyze the manifestation of correlation effects near the Fermi level. For that we compare in Fig. 2 LDA+DMFT [Fig. 2(a)] with DFT(LDA) [Fig. 2(b)] orbital-resolved density of states at the Fermi level $N(E_F)$ for all studied systems. The LDA+DMFT calculations show an increasing and pronounced dominance of $3d_{z^2}$ contribution at E_F along the series. This is in contrast to the DFT results where the Fe $3d_{z^2}$ orbital contribution also increases but is much lower and only significant for a -axis stretched CsFe_2As_2 with shortest

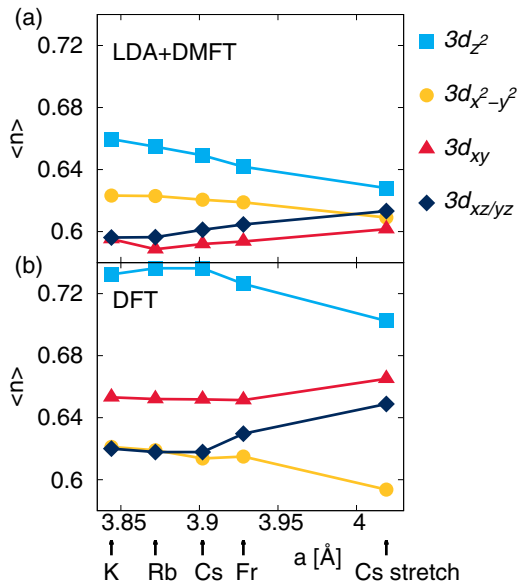


FIG. 3. (Color online) Filling of the Fe $3d$ orbitals as obtained from (a) LDA+DMFT and (b) DFT(LDA). Correlations reduce the overall Fe $3d$ filling, with the most correlated $3d_{xy}$ and $3d_{xz/yz}$ orbitals being the closest to half filling in contrast to the DFT result. Along the alkali metal series, the occupation of Fe $3d_{z^2}$ and $3d_{x^2-y^2}$ orbitals reduces, while that of the $3d_{xy}$ and $3d_{xz/yz}$ orbitals increases after a local minimum in RbFe_2As_2 , which has the smallest $3d_{xy}$ occupation of all systems studied.

As height. The nonmonotonous behavior of the Fe $3d_{xz/yz}$ contribution in DFT is a result of the special electronic structure of these systems at the M point. This feature is greatly suppressed by broadening effects in the LDA+DMFT calculation.

Linked to these results is the behavior of the LDA+DMFT orbitally-resolved electronic filling (see Fig. 3). We observe that inclusion of correlation effects not only reduces the overall Fe $3d$ filling due to the additional cost of the Coulomb interaction energy for doubly occupying a certain orbital, but also introduces orbital-dependent effects (see Sec. IID). While the Fe $3d_{z^2}$ and $3d_{x^2-y^2}$ filling decreases along the series, it increases for $3d_{xz/yz}$ and $3d_{xy}$.

C. Spectral function $A(\omega)$

In order to understand the origin of the changes in $N(E_F)$ and orbital filling, we show in Fig. 4 the local density of states [spectral function $A(\omega)$] for Fe $3d_{z^2}$ and Fe $3d_{xy}$ in the energy range $[-2, 2]$ eV for the representatives KFe_2As_2 , CsFe_2As_2 and a -axis stretched CsFe_2As_2 . We chose these two orbitals since they are the most affected along the series: $3d_{z^2}$ because of the decrease in As height from KFe_2As_2 to CsFe_2As_2 and $3d_{xy}$ because of the increase in the orbital localization with increasing a lattice parameter. Fe $3d_{z^2}$ shows a shift of orbital weight to negative energies (high binding energies) and a narrowing of the quasiparticlelike peak structure at E_F from KFe_2As_2 to CsFe_2As_2 . Since the electronic filling of the iron $3d$ orbitals is larger than half filling in these systems, the quasiparticlelike peak is located close to but below the Fermi level. In Fe $3d_{z^2}$ due to the reduction of the filling

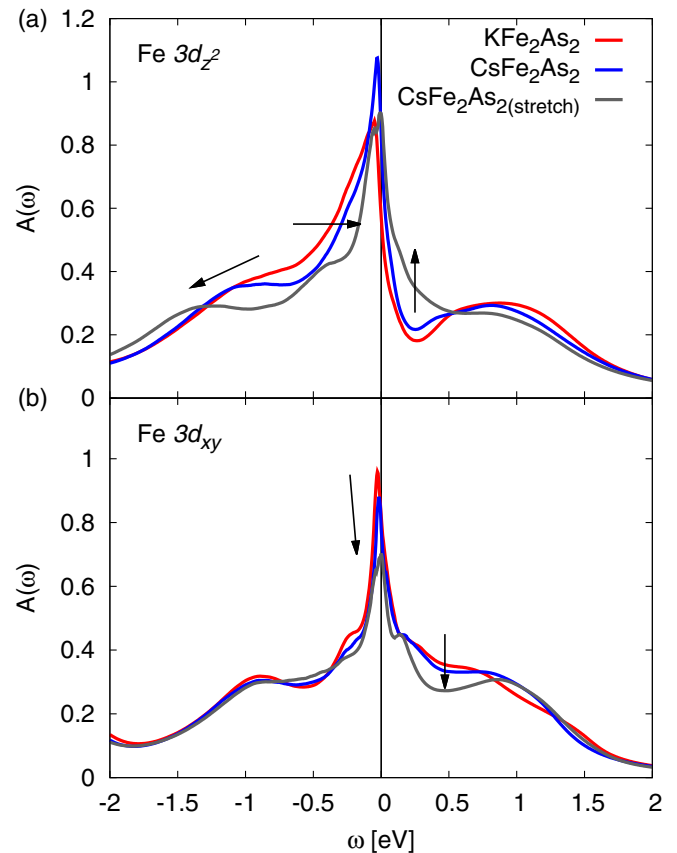


FIG. 4. (Color online) The density of states for (a) the Fe $3d_{z^2}$ orbital and (b) the Fe $3d_{xy}$ orbital as obtained from LDA+DMFT for the three compounds KFe_2As_2 , CsFe_2As_2 , and an a -axis stretched CsFe_2As_2 . Note the emergence of Hubbard-like peaks around -1.2 eV and $+1$ eV for $3d_{z^2}$ and around -1 eV and $+1$ eV for $3d_{xy}$. With arrows we mark the trend of the changes in the spectral function along the series.

from 0.66 in KFe_2As_2 to 0.63 in stretched CsFe_2As_2 (see Fig. 3) caused by an increase of electronic correlations, the quasiparticle peaklike structure is shifted even closer towards the Fermi level along the series, which in turn leads to the observed increase of the density of states at the Fermi level [Fig. 2(a)]. Such a shift of the quasiparticlelike peak structure in KFe_2As_2 was already noted in Ref. [34]. For the $3d_{xy}$ orbital, the quasiparticle peak is much closer to the Fermi level since the filling is closer to half filling at $n_{xy} \approx 0.59$. This orbital shows a strong suppression of the quasiparticle peak (up to $\approx 30\%$) from KFe_2As_2 to the a -axis stretched CsFe_2As_2 which points to an important increase of decoherence along the series. This increase of decoherence will be studied in more detail in the next section. Reduction of the maximum of the quasiparticle peak combined with a slight change of its position results in the almost constant density of states at the Fermi level for the $3d_{xy}$ orbital observed in Fig. 2(a).

Additionally, a shoulderlike feature appears in the spectral function at 1 eV and -1 eV in CsFe_2As_2 , closely resembling the typical spectral function shape of a quasiparticle peak and a lower and upper Hubbard band. These features do not correspond to any property found in the noninteracting DOS and are purely an effect of correlations and, at first sight, are

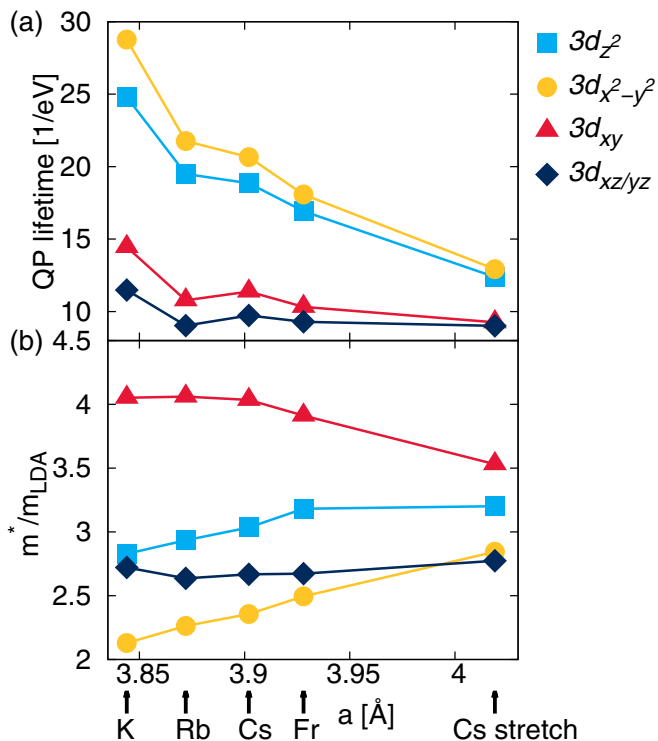


FIG. 5. (Color online) (a) Quasiparticle lifetimes given by $\tau_m = -(Z_m \text{Im} \Sigma_m(i0^+))^{-1}$ of the Fe $3d$ orbitals along the $A\text{Fe}_2\text{As}_2$ series and (b) the corresponding effective masses $\frac{m^*}{m_{\text{LDA}}}$.

similar to the emergence of Hubbard bands as a function of U in strongly correlated systems. This is also in agreement with the $3d_{xy}$ orbital being the strongest correlated one, whereas these features are far less developed in the $3d_{z^2}$ and other orbitals (see Appendix D). However, as we will show in Sec. II F, these peaks do not behave as expected for Hubbard bands in a one-band Hubbard model.

D. Effective masses and quasiparticle lifetimes

In order to quantify the change in correlation along the series $A\text{Fe}_2\text{As}_2$, we plot in Fig. 5 the orbitally resolved quasiparticle lifetimes and effective masses $\frac{m^*}{m_{\text{LDA}}}$. The effective masses for Fe $3d_{z^2}$ and $3d_{x^2-y^2}$ increase along the $A\text{Fe}_2\text{As}_2$ series but remain constant or even slightly decrease for $3d_{xz/yz}$ and $3d_{xy}$. This last result cannot be explained solely by the behavior of the DFT-derived tight binding parameters (see Appendices B and C).

Information on the origin of this behavior can be obtained from the quasiparticle lifetimes which strongly decrease for all orbitals along the series [Fig. 5(a)]. This indicates that the coherent quasiparticle picture, being the basis for the calculation of the effective masses, becomes less appropriate along the $A\text{Fe}_2\text{As}_2$ series, and accordingly, the effective masses obtained by this procedure are an underestimation of the true value. This result shows that already at the temperature of $T = 145$ K these systems are quite incoherent. With increasing lattice parameter incoherence significantly increases, albeit leading to an orbital dependent change in localization of the Fe $3d$ electrons. In particular, we find a pro-

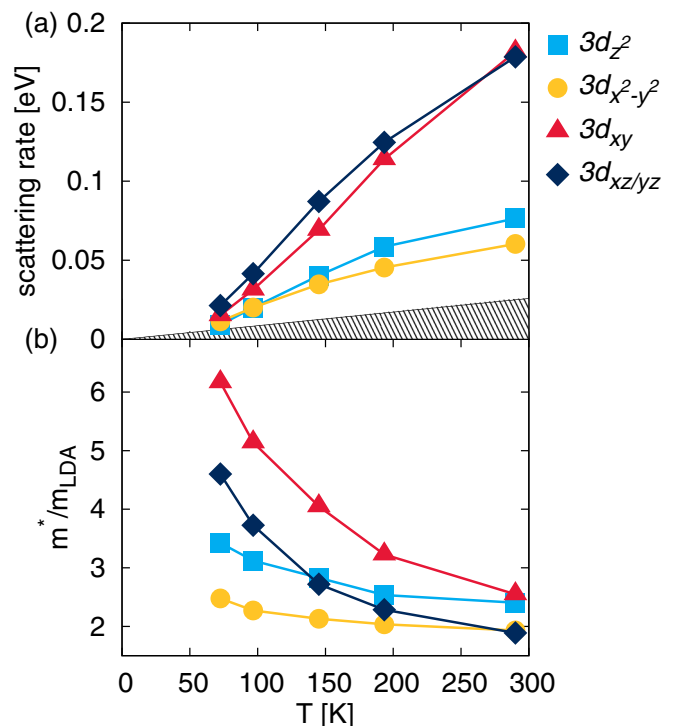


FIG. 6. (Color online) Temperature dependence of the (a) scattering rates $-Z_m \text{Im} \Sigma_m(i0^+)$ of the Fe $3d$ orbitals of KFe_2As_2 . The shaded area indicates the coherent domain. The coherence temperature estimate T^* as deduced from the scattering rate is quite low, located around 50 K. (b) The corresponding effective masses.

nounced decrease of the quasiparticle lifetime from KFe_2As_2 to RbFe_2As_2 , which we attribute to the competing effects of decrease of Fe-Fe direct hopping and increase in Fe-Fe indirect hopping through As, which seem to have a crossover point between RbFe_2As_2 and CsFe_2As_2 (see Appendix B).

In Fig. 6 we show the temperature dependence of the quasiparticle scattering rates and effective masses of KFe_2As_2 . We find a similar temperature dependence as also observed for multiorbital SrRuO_3 and CaRuO_3 in Ref. [46]. As the temperature is lowered in the calculation, the quasiparticle picture, which is suppressed at high temperatures, is partially restored, leading to an exponential increase in the quasiparticle lifetimes. Still, even at the lowest studied temperature of $T = 72$ K the width (scattering rate) of the quasiparticle peak $-Z_m \text{Im} \Sigma_m(i0^+)$ is still larger than the temperature, indicating that coherent quasiparticle excitations are still in the minority. From our results for the scattering rate we estimate that the temperature T^* for the incoherent-coherent phase transition for our chosen interaction parameters $U = 4$ eV, $J_H = 0.8$ eV is around 50 K, and it is even lower for RbFe_2As_2 and CsFe_2As_2 . This is in qualitative agreement with previous LDA+DMFT estimates for KFe_2As_2 [34] and with magnetic susceptibility and thermal expansion measurements which predict the coherence scale of KFe_2As_2 to be around 100 K [27,29,36] and even lower for RbFe_2As_2 and CsFe_2As_2 [20,36]. We expect that inclusion of the full rotationally invariant Hund's coupling, which is beyond the scope of the present paper, will shift the transition to higher temperatures in the calculation [2,3,47] and, therefore, closer to experiment. The consequences of

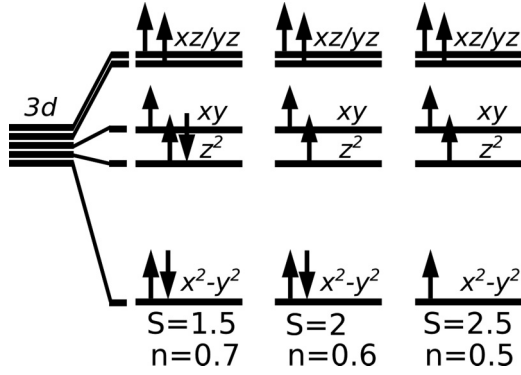


FIG. 7. Sketch of some of the most likely Fe atomic orbital configurations in hole-doped 122 iron pnictide systems. The electronic filling is indicated by n and the total spin by S .

inclusion of rotationally invariant interactions have been extensively discussed in previous papers in the framework of the two-band [48] and three-band [49] Hubbard models. The computational effort of including these terms in the five-band cases studied here is beyond the scope of the present paper. However, we performed some benchmarking calculations with fully rotational Hund's coupling and find that the coherence transition shifts to higher temperatures as found in other studies [2,3,47]. In this sense the presented results can be considered as a lower bound to the experimental observations.

The increase of effective masses at lower temperatures in our calculation is precisely the effect of restoring the coherent quasiparticle picture, so that the effective masses at the lowest temperature (72 K) we investigated can be considered as the closest approximation to the true values, i.e., 6.1 ($3d_{xy}$), 4.6 ($3d_{xz/yz}$), 3.4 ($3d_{z^2}$) and 2.5 ($3d_{x^2-y^2}$). Combining these observations along the series we conclude that alkali 122 systems show typical signs of strong correlations but, in the studied range of temperatures, are actually quite deep in the incoherent bad metal region with a well defined, albeit strongly suppressed, quasiparticle peak.

E. Nature of the Fe 3d wave function

We proceed now with an analysis of the wave function in terms of the Fe atomic basis states, similar to what has been done for other pnictide systems [2,4]. In Fig. 7 we show a sketch for a few typical orbital configurations in these systems with the orbital splittings obtained from the downfolded charge self-consistent LDA Hamiltonian. Since the nominal electronic filling for Fe 3d for these systems is 5.5 electrons per Fe, one would expect atomic Fe 3d states with 5 and 6 electrons to be the most likely states. However, as shown in Fig. 3, the actual average Fe 3d filling is slightly larger than 6/10, and this can be analyzed in the histogram of Fig. 7. For the interacting system there is a nontrivial competition between the energy contribution due to the crystal field splitting, which prefers to occupy the lowest states first, the on-site U interaction, which tends to decrease the filling of the localized states, and the Hund's coupling J_H , which prefers orbital states with maximum total spin. When the Hund's coupling J_H is large compared to the total crystal field splitting, the high-spin states will have the highest probability

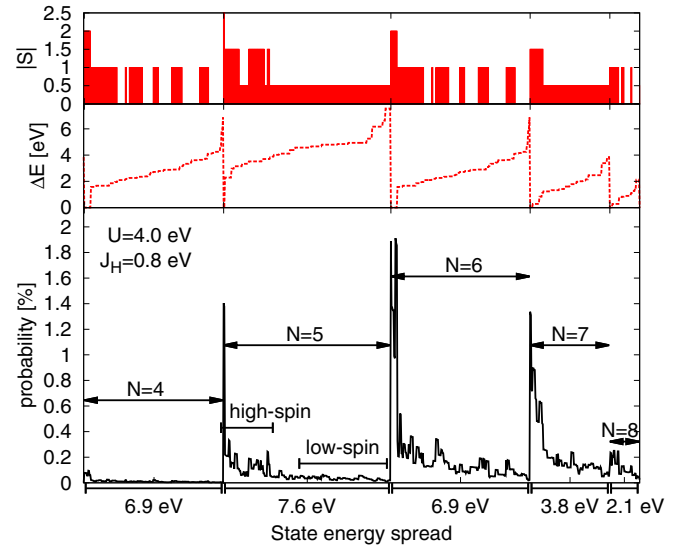


FIG. 8. (Color online) The histogram of the Fe 3d atomic state for KFe_2As_2 at $T = 145$ K. The probability corresponds to the fraction of time the Fe 3d orbitals spend in one of the $2^{10} = 1024$ possible states. Within the interval of constant electron number N the states are sorted by increasing energy, i.e., the leftmost states within an interval correspond to high-spin states, while the rightmost states correspond to low-spin states.

and the low-spin states will be suppressed. This is indeed true for the hole-doped 122 iron pnictides.

In Fig. 8 we show for KFe_2As_2 the atomic histogram of the Fe 3d shell, i.e., the projection of the wave function onto the Fe 3d atomic basis states. The states are sorted by the number of electrons N , and inside the interval of constant filling the states are sorted by energy. Because of the Hund's coupling, the leftmost states in such an interval correspond to the high-spin states, while the rightmost states correspond to low-spin states. The probability assigned to each state corresponds to the fraction of time in the calculation the 3d orbitals spend in a specific configuration. Due to the Hund's coupling the high-spin states clearly dominate the histogram, although their probabilities are quite low with less than 2%. Even for the low-spin states at higher energy the probability, while being smaller, is never close to zero, which causes the Fe 3d orbitals to visit a large number of accessible states over time even when they are much higher in energy. Since all these states contribute with a finite fraction to the Fe 3d spectral function, no well defined atomiclike excitations can be expected. This leads to the observed suppression of the quasiparticle peak and subtle high-binding energy features in the spectral function without well defined Hubbard bands, which is the distinctive property of Hund's metals [4,15].

This behavior becomes even more pronounced when we perform this analysis along the AFe_2As_2 series. In Fig. 9(a) we analyze the most likely atomic states from the histogram of the Fe 3d orbitals for AFe_2As_2 . For all systems, six out of the seven most likely atomic states are solely composed of the maximal high-spin states with $S = 2.5$ and $S = 2$. For the earth alkali (undoped) 122 iron pnictides like BaFe_2As_2 the atomic ground state of the Fe atom with a valence charge of 6 has a maximum possible spin of $S = 2$. Since for the systems studied here one

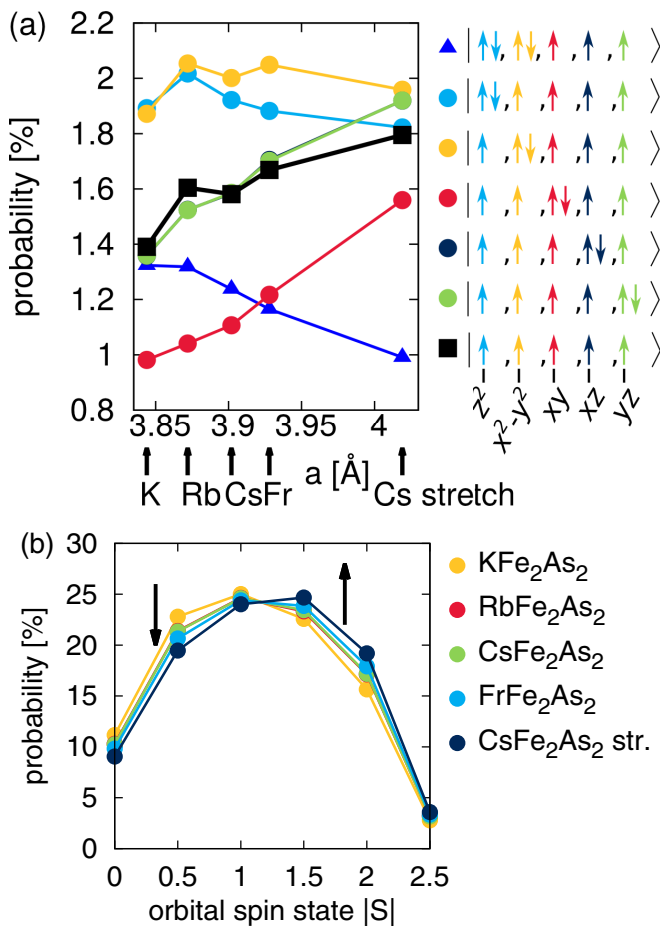


FIG. 9. (Color online) (a) Probabilities of the most likely atomic states of the Fe 3d atomic orbitals for the $A\text{Fe}_2\text{As}_2$ series. The probability corresponds to the fraction of time the atom in the DMFT calculation spends in a specific state. (b) The summed probability of all atomic states with a given total spin S . High-spin states become more likely for increasing lattice parameter a , while the probability of low-spin states is reduced.

electron per formula unit has been removed by hole doping, the probability for the fully polarized half-filled $S = 2.5$ state with 5 electrons in the Fe 3d orbitals is among the most likely states with a comparably high probability of 1.4% (or 2.8% when accounting for spin degeneracy) in KFe_2As_2 , that increases up to 1.8% (or 3.6%) in the stretched CsFe_2As_2 system. Along the series the low-spin states become suppressed while the high-spin states increase in probability, as can be seen in Fig. 9(b).

Generally, the systems can reduce their energy by assigning a higher probability to high-spin states due to the Hund's coupling J_H . This leads to a significant increase of localization caused by the orbital blocking mechanism [4]. Since J_H enforces a high-spin state, orbital mixing is greatly suppressed compared to a vanishing Hund's coupling where high- and low-spin states would have equal energies and, therefore, probabilities. This is the typical behavior of a so-called Hund's metal, in which the electronic correlations are much more sensitive to the value of J_H than to the on-site Coulomb term U . Therefore, in the hole-doped end systems like CsFe_2As_2 and especially the a -axis stretched CsFe_2As_2 , the Hund's coupling becomes the most important interaction that governs the physical properties of these systems.

F. Dependence on U and J_H

In order to investigate the effects of U and J_H more explicitly and to determine the nature of the peak/shoulder at $[-1.5, -1]$ eV, we performed calculations for different interaction parameters for the most correlated case, the a -axis stretched CsFe_2As_2 system. For computational efficiency these calculations were done at higher temperature $\beta = 40 \text{ eV}^{-1}$. While the height of the quasiparticle peak is reduced at higher temperatures, the behavior of the spectral function at $[-2, -1]$ eV is quite robust. We considered on-site Coulomb values $U = 4, 5,$ and 6 eV and Hund's couplings of $J_H = 0.8, 1.0,$ and 1.2 eV . In Figs. 10 and 11 we show the spectral function $A(\omega)$ for Fe $3d_{z^2}$ and $3d_{xy}$. An increase of U from 4 eV to 6 eV

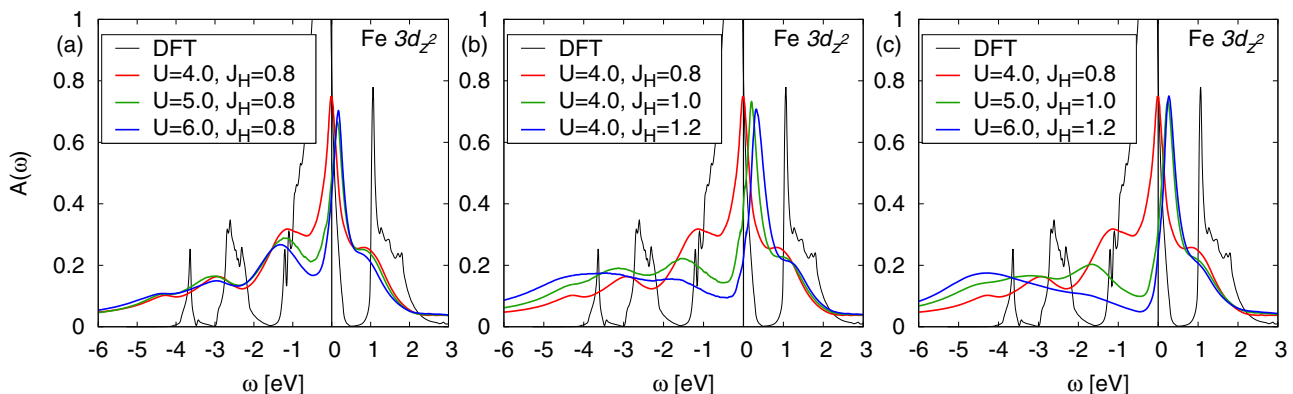


FIG. 10. (Color online) The density of states for the Fe $3d_{z^2}$ orbital of the stretched CsFe_2As_2 compound as a function of the on-site Coulomb repulsion U and Hund's coupling J_H . (a) An increase only in U leads to an increase in renormalization, i.e., effective masses and a pronounced Hubbard-like peak at -1.5 eV but no other qualitative changes are observed. (b) The Hund's coupling J_H greatly increases the decoherence of the electronic states at the Fermi level and leads to a significant shift of spectral weight down to lower energies. (c) The combined effect of U and J_H is qualitatively very similar to an increase in J_H alone.

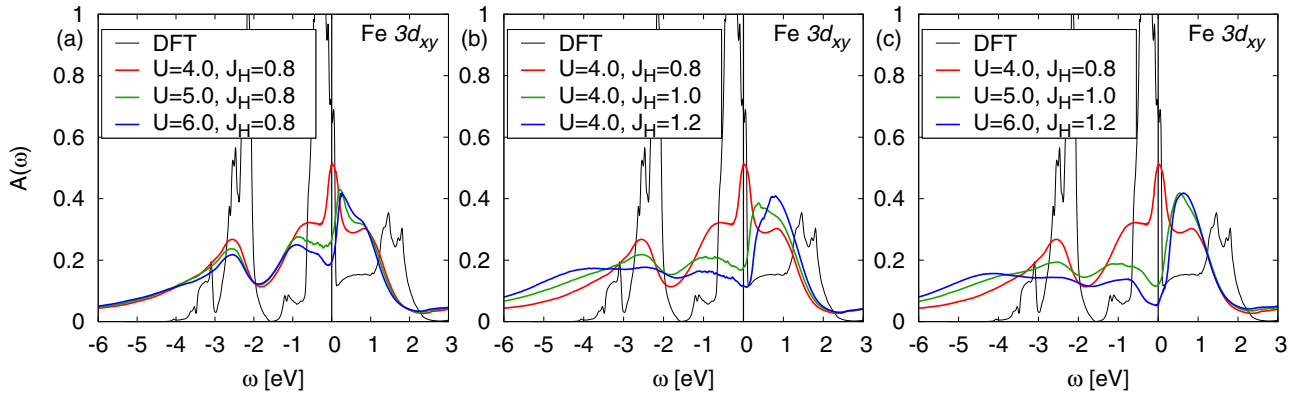


FIG. 11. (Color online) The density of states for the Fe $3d_{xy}$ orbital of the stretched CsFe_2As_2 compound as a function of the on-site Coulomb repulsion U and Hund's coupling J_H . Similar to the Fe $3d_{z^2}$ orbital, we see that the shift of spectral weight to lower energies is almost exclusively dependent on the Hund's coupling J_H . Being the most correlated orbital, the DOS of the Fe $3d_{xy}$ orbital at the Fermi level is almost gapped for $U = 6$ eV and $J_H = 1.2$ eV.

at a fixed J_H implies only moderate changes in the spectral function in general for all Fe $3d$ orbitals. The Hubbard-like shoulder at -1.2 eV becomes more pronounced for larger U values, and its maximum moves only very slightly to negative energies (-1.4 eV). Due to particle-hole asymmetry, we obtain a quasiparticlelike peak slightly shifted away from the Fermi level. On the other hand, an increase in the Hund's coupling J_H for fixed U immediately renders the system very incoherent, with a strong increase in the scattering rate and a reduction of the quasiparticle lifetime, leading to a strong suppression of DOS at the Fermi level and a significant shift of spectral weight to lower energies, forming a broad lower Hubbard band located between -4 and -5 eV. Finally, the combined effect of U and J_H yields an even more well defined lower Hubbard-like band at around -4.5 eV. While this characteristic dependence on U and J_H is very similar for all Fe $3d$ orbitals, we still find a strong orbital selection regarding the remaining spectral weight at the Fermi level. The Fe $3d_{xy}$ orbital especially is almost gapped at the Fermi level for the largest interaction values considered (see Fig. 11), while the least correlated Fe $3d_{x^2-y^2}$ orbital experiences basically no suppression of the DOS at the Fermi level regardless of the interaction parameters and instead retains a well defined quasiparticle peak for higher values of U and J_H (see Appendix D). We also checked the case of negligible Hund's coupling by setting $J_H = 0$, which recovered the coherence properties even at $T = 300$ K, with low effective masses around 1.4 and a spectral function that resembled quite well the DFT density of states.

Our results confirm the general picture of the iron pnictides being "Hund's metals" with strong orbital separation, especially for the strongly correlated hole-doped end systems considered in this study. In this case, a slight increase of J_H renders the system much more incoherent and "bad metal"-like for the same value of U , while the spectral weight at the Fermi level differs strongly between the orbitals but remains finite even for larger values of U .

III. CONCLUSIONS

From our analysis of the electronic properties within LDA+DMFT in a wide range of binding energies, we conclude

that along the isoelectronic doping series $A\text{Fe}_2\text{As}_2$ ($A = \text{K}, \text{Rb}, \text{Cs}$) as well as the fictitious FrFe_2As_2 and a -axis stretched CsFe_2As_2 , which shows a monotonous increase of the a lattice parameters and a decrease of the As z height, correlation and incoherence of the Fe $3d$ orbitals increase, albeit orbitally selective, and the systems show clear features of a Hund's metal. In this case the Hund's coupling plays the major role and renders these materials much more incoherent than expected from the value of the Coulomb repulsion U alone. While the most correlated orbitals (d_{xy}) show features that resemble those of being close to an orbital selective Mott transition, especially for a -stretched CsFe_2As_2 , the system is quite deep in the incoherent bad metal regime with a finite spectral weight at the Fermi level even for $U = 6$ eV and $J_H = 1.2$ eV. Experimentally, we predict that an increase of the Fe-Fe distance in CsFe_2As_2 by stretching will induce an orbital dependent increase in correlations and incoherence of the Fe $3d$ orbitals, where the Fe $3d_{z^2}$ and Fe $3d_{xy}$ orbitals are strongly but not fully localized and the other Fe $3d$ orbitals retain a bad metallic behavior. From our results we estimate the coherence temperature to be located around 50 K in KFe_2As_2 and even lower for RbFe_2As_2 and CsFe_2As_2 in qualitative agreement with the experimental observations. These features make the hole doped end systems of the 122 iron pnictides, namely KFe_2As_2 , RbFe_2As_2 , and especially CsFe_2As_2 and a -axis stretched CsFe_2As_2 , a valuable test bed to study the behavior of strongly correlated Hund's metals and orbital-selective bad metallicity and its interplay with superconductivity.

ACKNOWLEDGMENTS

The authors would like to thank Felix Eilers, Kai Grube, Frédéric Hardy, Christoph Meingast, Leni Bascones, Bernd Büchner, Stefan-Ludwig Drechsler, and Aaram J. Kim for fruitful discussions and gratefully acknowledge the Deutsche Forschungsgemeinschaft for financial support through Grant No. SPP 1458.

APPENDIX A: METHODS

For our fully charge self-consistent LDA+DMFT calculations (see Ref. [33] for detailed explanation) we use

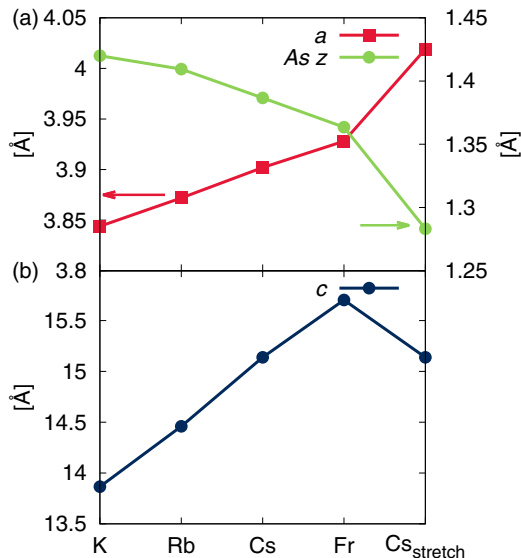


FIG. 12. (Color online) The structural parameters for the considered materials KFe_2As_2 (K), RbFe_2As_2 (Rb), CsFe_2As_2 (Cs) (from Ref. [45]) and the fictitious systems FrFe_2As_2 (Fr) and stretched CsFe_2As_2 ($\text{Cs}_{\text{stretch}}$). (a) The a parameter and absolute height of the As atom above the Fe plane. (b) The c -lattice parameter.

the structural parameters from Ref. [45] for the tetragonal structures of KFe_2As_2 , RbFe_2As_2 , and CsFe_2As_2 at room temperature. Due to the almost perfect linear dependence of the lattice parameters as a function of atomic radius, we further use linear extrapolation to obtain structural parameters for fictitious FrFe_2As_2 , avoiding possible ambiguities from DFT-based relaxation methods which do not work satisfactorily for these systems. Additionally, we prepare a structure for CsFe_2As_2 that is extended along the a/b axis by 3% and has a reduced relative As z height of 2% to mimic a small expansion of the lattice. The expansion is performed in both the x and y direction so that tetragonal symmetry is preserved. The lattice parameters and As z position are shown in Fig. 12.

For the DFT calculations we used the WIEN2K [50] implementation of the full-potential linear augmented plane wave (FLAPW) method in the local density approximation. The Kohn-Sham equations were solved on 726 k points in the irreducible Brillouin zone, resulting in a $21 \times 21 \times 21$ k mesh in the conventional Brillouin zone. A local orbital basis was obtained by a projection of the Bloch wave functions to the localized Fe $3d$ orbitals, using our implementation of the method described in Refs. [9,51]. Please note that a coordinate system which is rotated by 45° around the z axis with respect to the conventional $I4/mmm$ unit cell is used. Thus, the x and y axis point towards neighboring Fe atoms. The energy window for the bands to be considered for projection was chosen to be $[-6, 13]$ eV, with the lower boundary lying in a gap in the density of states (DOS). Consequently, 35 bands on average were taken into account for the projection, resulting in a representation of the k -dependent and local noninteracting spectral function for each orbital that is indistinguishable from the DFT result in the chosen energy window.

The DMFT impurity problem was solved with the continuous-time quantum Monte Carlo method in the hy-

bridization expansion [52] as implemented in the ALPS [53,54] project. In the calculations we used an inverse temperature of $\beta = 80 \text{ eV}^{-1}$, corresponding to the temperature of 145 K, unless stated differently. A total number of at least 50×10^6 Monte-Carlo sweeps were performed for each solution of the impurity model and up to 90×10^6 sweeps for the larger interaction parameters. For the double counting correction we used the nominal double counting [55,56], which has been shown to yield significantly better agreement with photoemission experiments [56], especially for low and high binding energies, while other methods like the FLL [57,58] double counting scheme overestimate the valence charge and underestimate a possible Mott gap [56]. The interaction parameters were used in the definition of the Slater integrals [59] F^k with $U = F^0$ and $J_H = (F^2 + F^4)/14$. For the on-site Coulomb interaction we considered a value of $U = 4 \text{ eV}$ and for Hund's rule coupling $J_H = 0.8 \text{ eV}$, unless stated differently. We calculate the effective masses directly from the impurity self-energy via

$$\frac{m^*}{m_{\text{LDA}}} = 1 - \left. \frac{\partial \text{Im}\Sigma(i\omega)}{\partial \omega} \right|_{\omega \rightarrow 0^+}, \quad (\text{A1})$$

with the quasiparticle weight being defined as the inverse of the effective mass $Z = \left[\frac{m^*}{m_{\text{LDA}}} \right]^{-1}$. The continuation of the Monte Carlo data to the real axis was done by stochastic analytic continuation [60]. For obtaining the hopping matrix elements we obtained a tight-binding Hamiltonian from projective Wannier functions [61] from DFT, generated by the all-electron full-potential local orbital (FPLO) [62] code, using a 10 (16) orbital model, including the Fe $3d$ only (10-orbital model) [63] or Fe $3d$ and As $4p$ orbitals (16-orbital model).

APPENDIX B: 10-BAND TIGHT BINDING MODEL

In order to quantify at the level of DFT the effects of negative pressure introduced by isovalent doping in AFe_2As_2 ($A = \text{K, Rb, Cs, Fr}$), we calculated the Fe-Fe hopping matrix elements via projective Wannier functions. The absolute values of the hopping parameters are plotted in Fig. 13. There are two main contributions that affect the values of the Fe-Fe hopping parameters: First, the increase of the interatomic distances due to increasing atomic radii of the alkali ions implies a decrease of the direct Fe-Fe hopping. Second, due to elongation of the Fe-As tetrahedron, the As atom moves closer to the Fe-Fe plane. This reduction of the As $_z$ height leads to an increase of the indirect hopping along the path Fe-As-Fe. The total contribution of these two effects translates into a nontrivial behavior of the Fe-Fe effective hoppings along the doping series (K,Rb,Cs)Fe $_2$ As $_2$. The Fe $3d_{xy}$ -Fe $3d_{xy}$ effective hopping is the smallest in KFe_2As_2 due to the almost perfect cancellation of the two contributions as pointed out in Ref. [4]. As the lattice parameter increases, the indirect Fe-As-Fe hopping contribution outweighs the contribution coming from the direct Fe-Fe orbital overlap. This causes a slight increase of the hopping parameters from KFe_2As_2 to CsFe_2As_2 . These two contributions are very similar for hoppings between Fe $3d_{xz/yz}$ orbitals. The trend in the hoppings between Fe $3d_{z^2}$ and $3d_{x^2-y^2}$ orbitals is less affected by changes of the indirect hopping contribution and shows a small overall decrease in the hopping to the neighboring Fe $3d$ orbitals.

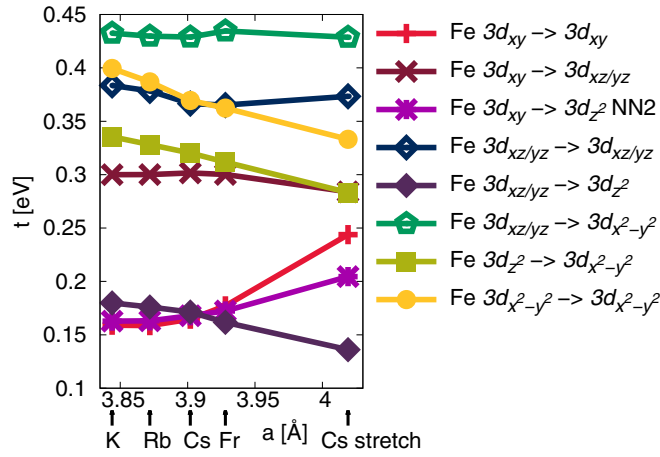


FIG. 13. (Color online) Eight largest effective Fe-Fe hopping parameters t obtained from a 10-band tight binding fit. Also shown are some second nearest neighbor parameters indicated by the label NN2. The nontrivial evolution of the hopping values with increasing lattice parameter and reduced As_z height leads to different degrees of localization and effects of correlation in the Fe $3d$ orbitals along the series KFe_2As_2 , RbFe_2As_2 , CsFe_2As_2 , and FrFe_2As_2 .

APPENDIX C: 16-BAND TIGHT BINDING MODEL

In Fig. 14 we show the six largest Fe-Fe hopping parameters obtained from a 16-band tight binding fit, encompassing the Fe $3d$ and As $4p$ orbitals. The overall monotonous decrease resembles the increase of the interatomic distance that leads to a reduced overlap of the neighboring Fe $3d$ orbitals. As noted in the main text, the indirect hopping through the As $4p$ orbitals has an important effect on the effective hopping parameters. Taking only the direct Fe-Fe hopping into account, we observe the expected decrease of the hopping parameters which resembles the reduced hybridization as the lattice parameters are increased. In combination with the indirect hopping via the As atom, this leads to a nontrivial behavior of the effective hopping parameters.

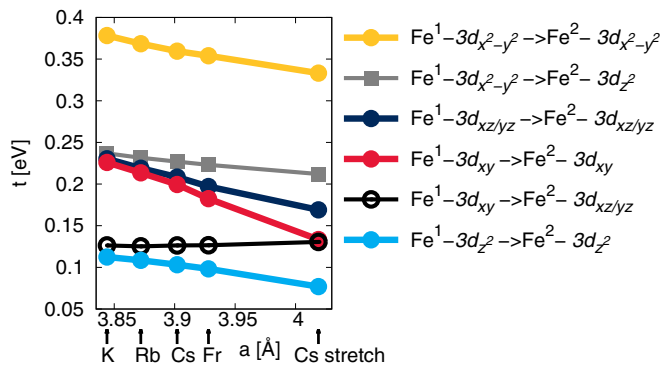


FIG. 14. (Color online) The first six largest hopping parameters t for the Fe-Fe hopping obtained from a 16-band tight binding fit. Fe^i denotes the i th atom out of the two equivalent iron atoms in the irreducible Brillouin zone.

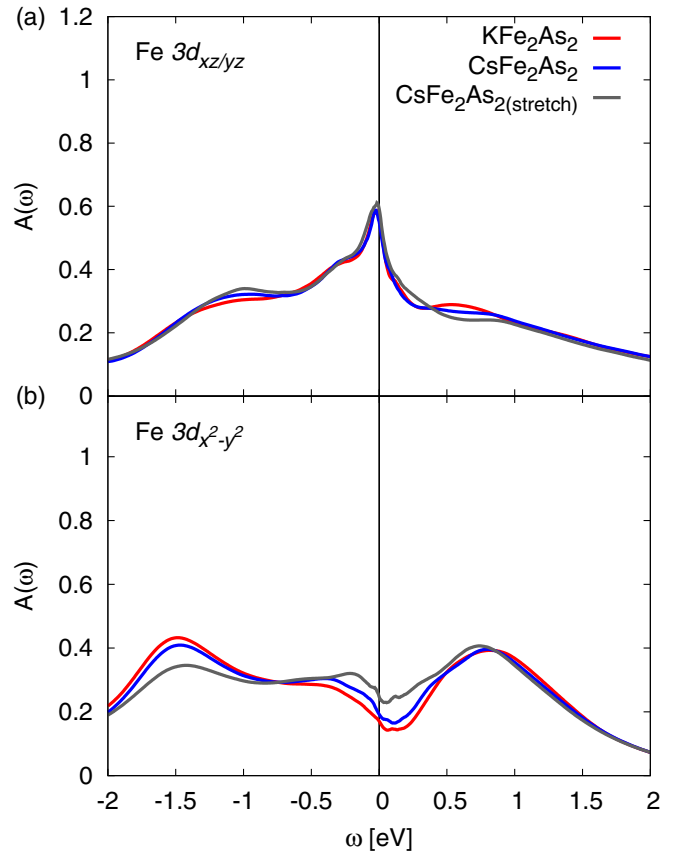


FIG. 15. (Color online) The density of states for (a) the Fe $3d_{xz/yz}$ orbital and (b) the Fe $3d_{x^2-y^2}$ orbital for $U = 4$ eV and $J_H = 0.8$ eV as obtained from LDA+DMFT for the three compounds KFe_2As_2 , CsFe_2As_2 , and an expanded structure of CsFe_2As_2 .

APPENDIX D: DOS FOR OTHER ORBITALS

In Fig. 15 we show the local spectral function of the Fe $3d_{xz/yz}$ and $3d_{x^2-y^2}$ orbital for KFe_2As_2 , CsFe_2As_2 , and a -axis stretched CsFe_2As_2 . Compared to the other Fe $3d$ orbitals they are less affected by an increase of the lattice parameter a . Similar to the $3d_{z^2}$ and $3d_{xy}$ orbital a small Hubbard-like peak becomes more pronounced in the $3d_{xz/yz}$ orbital, while the $3d_{x^2-y^2}$ orbital shows the opposite trend, increasing its spectral function at the Fermi level at the cost of decreasing it at negative energies.

In Fig. 16 we show the dependence of the Fe $3d_{xz/yz}$ and $3d_{x^2-y^2}$ orbital spectral function on U and J_H . The results are very similar to the other orbitals, with the effect of increasing U being much less extreme than that of J_H . While at higher U the spectral function still mimics the LDA result, an increase in J_H results in a large shift of spectral weight to negative energies. The $3d_{x^2-y^2}$ orbital shows the smallest degree of correlations and is the only orbital that retains a well defined quasiparticle peak at the Fermi level even for larger interaction parameters.

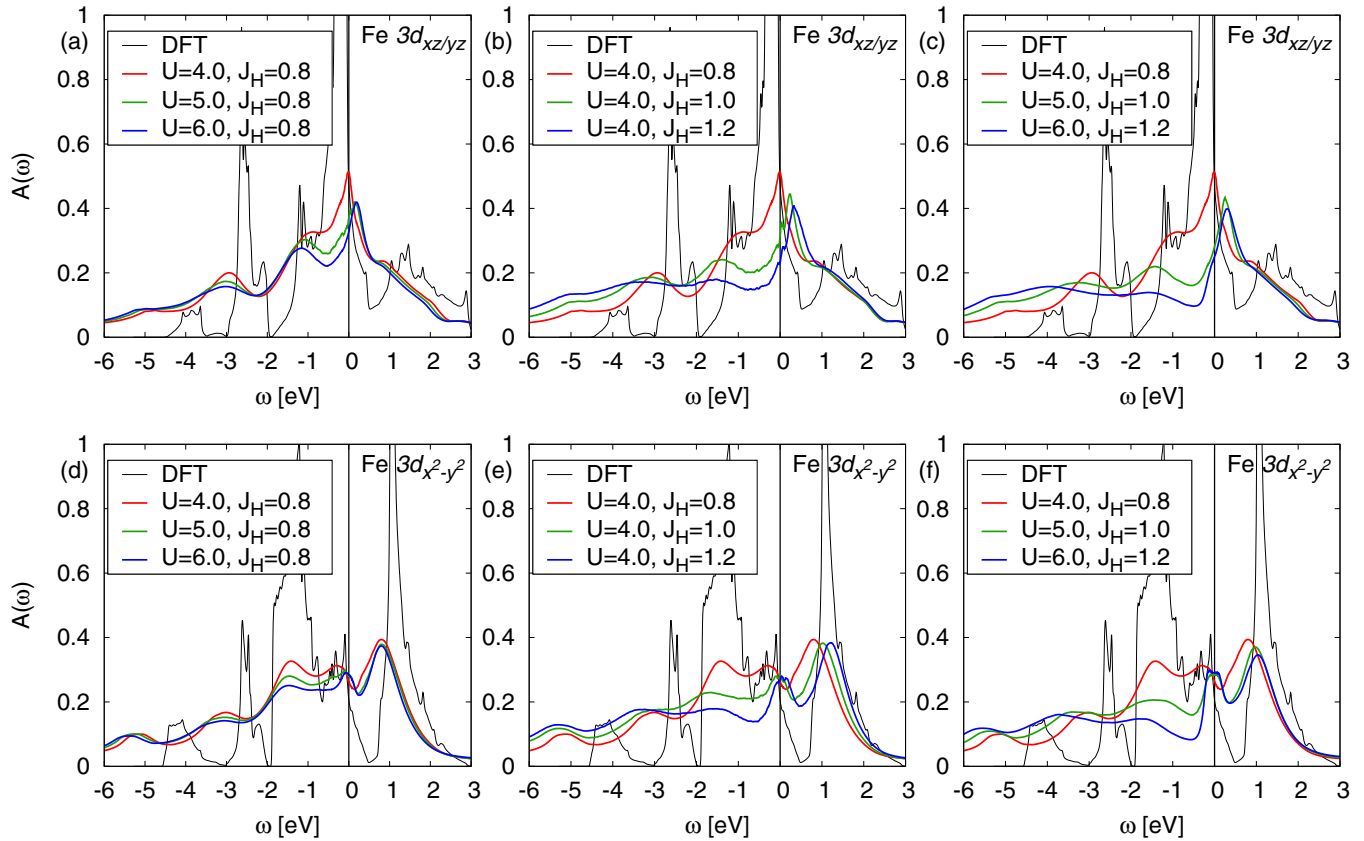


FIG. 16. (Color online) The density of states for the Fe $3d_{xz/yz}$ and $3d_{x^2-y^2}$ orbital of the stretched CsFe_2As_2 compound as a function of the on-site Coulomb repulsion U and Hund's coupling J_H . (a),(d) An increase only in U leads to a slightly better pronounced lower Hubbard bandlike feature but otherwise no qualitative changes to the high energy features. (b),(e) The Hund's coupling J_H greatly increases the decoherence of the electronic states at the Fermi level and leads to a significant shift of spectral weight down to negative energies. (c),(f) The combined effect of U and J_H is qualitatively very similar to an increase in J_H alone.

- [1] Y. Kamihara, T. Watanabe, M. Hirano, and H. Hosono, Iron-based layered superconductor $\text{La}[\text{O}_{1-x}\text{F}_x]\text{FeAs}$ ($x = 0.05 - 0.12$) with $T_c = 26$ K, *J. Am. Chem. Soc.* **130**, 3296 (2008).
- [2] K. Haule and G. Kotliar, Coherence-incoherence crossover in the normal state of iron oxypnictides and importance of Hund's rule coupling, *New J. Phys.* **11**, 025021 (2009).
- [3] M. Aichhorn, S. Biermann, T. Miyake, A. Georges, and M. Imada, Theoretical evidence for strong correlations and incoherent metallic state in FeSe, *Phys. Rev. B* **82**, 064504 (2010).
- [4] Z. P. Yin, K. Haule, and G. Kotliar, Kinetic frustration and the nature of the magnetic and paramagnetic states in iron pnictides and iron chalcogenides, *Nat. Mater.* **10**, 932 (2011).
- [5] L. de' Medici, J. Mravlje, and A. Georges, Janus-Faced Influence of Hund's Rule Coupling in Strongly Correlated Materials, *Phys. Rev. Lett.* **107**, 256401 (2011).
- [6] R. Yu and Q. Si, Mott transition in multiorbital models for iron pnictides, *Phys. Rev. B* **84**, 235115 (2011).
- [7] J. Ferber, H. O. Jeschke, and R. Valentí, Fermi Surface Topology of LaFePO and LiFeP , *Phys. Rev. Lett.* **109**, 236403 (2012).
- [8] J. Ferber, K. Foyevtsova, R. Valentí, and H. O. Jeschke, LDA + DMFT study of the effects of correlation in LiFeAs , *Phys. Rev. B* **85**, 094505 (2012).
- [9] M. Aichhorn, L. Pourovskii, V. Vildosola, M. Ferrero, O. Parcollet, T. Miyake, A. Georges, and S. Biermann, Dynamical mean-field theory within an augmented plane-wave framework: Assessing electronic correlations in the iron pnictide LaFeAsO , *Phys. Rev. B* **80**, 085101 (2009).
- [10] A. Liebsch, High-energy pseudogap induced by Hund coupling in a degenerate Hubbard model, *Phys. Rev. B* **84**, 180505(R) (2011).
- [11] A. Georges, L. de' Medici, and J. Mravlje, Strong correlations from Hund's coupling, *Annu. Rev. Condens. Matter Phys.* **4**, 137 (2013).
- [12] L. de' Medici, G. Giovannetti, and M. Capone, Selective Mott Physics as a Key to Iron Superconductors, *Phys. Rev. Lett.* **112**, 177001 (2014).
- [13] Y. X. Yao, J. Schmalian, C. Z. Wang, K. M. Ho, and G. Kotliar, Comparative study of the electronic and magnetic properties of BaFe_2As_2 and BaMn_2As_2 using the Gutzwiller approximation, *Phys. Rev. B* **84**, 245112 (2011).

- [14] R. Yu and Q. Si, Orbital-Selective Mott Phase in Multiorbital Models for Alkaline Iron Selenides $K_{1-x}Fe_{2-y}Se_2$, *Phys. Rev. Lett.* **110**, 146402 (2013).
- [15] L. Fanfarillo and E. Bascones, Electronic correlations in Hund metals, *Phys. Rev. B* **92**, 075136 (2015).
- [16] J. Paglione and R. L. Greene, High-temperature superconductivity in iron-based materials, *Nat. Phys.* **6**, 645 (2010).
- [17] A. E. Böhmer, F. Hardy, L. Wang, T. Wolf, P. Schweiss, and C. Meingast, Superconductivity-induced re-entrance of the orthorhombic distortion in $Ba_{1-x}K_xFe_2As_2$, *Nat. Commun.* **6**, 7911 (2015).
- [18] X. C. Hong, X. L. Li, B. Y. Pan, L. P. He, A. F. Wang, X. G. Luo, X. H. Chen, and S. Y. Li, Nodal gap in iron-based superconductor $CsFe_2As_2$ probed by quasiparticle heat transport, *Phys. Rev. B* **87**, 144502 (2013).
- [19] Z. Zhang, A. F. Wang, X. C. Hong, J. Zhang, B. Y. Pan, J. Pan, Y. Xu, X. G. Luo, X. H. Chen, and S. Y. Li, Heat transport in $RbFe_2As_2$ single crystals: Evidence for nodal superconducting gap, *Phys. Rev. B* **91**, 024502 (2015).
- [20] F. Eilers, Ph.D. thesis, Karlsruhe, 2014.
- [21] K. Kihou, T. Saito, S. Ishida, M. Nakajima, Y. Tomioka, H. Fukazawa, Y. Kohori, T. Ito, S. Uchida, A. Iyo, C. Lee, and H. Eisaki, Single Crystal Growth and Characterization of the Iron-Based Superconductor KFe_2As_2 Synthesized by KAs Flux Method, *J. Phys. Soc. Jpn.* **79**, 124713 (2010).
- [22] J. K. Dong, S. Y. Zhou, T. Y. Guan, H. Zhang, Y. F. Dai, X. Qiu, X. F. Wang, Y. He, X. H. Chen, and S. Y. Li, Quantum Criticality and Nodal Superconductivity in the FeAs-Based Superconductor KFe_2As_2 , *Phys. Rev. Lett.* **104**, 087005 (2010).
- [23] A. F. Wang, B. Y. Pan, X. G. Luo, F. Chen, Y. J. Yan, J. J. Ying, G. J. Ye, P. Cheng, X. C. Hong, S. Y. Li, and X. H. Chen, Calorimetric study of single-crystal $CsFe_2As_2$, *Phys. Rev. B* **87**, 214509 (2013).
- [24] H. Ding, P. Richard, K. Nakayama, K. Sugawara, T. Arakane, Y. Sekiba, A. Takayama, S. Souma, T. Sato, T. Takahashi, Z. Wang, X. Dai, Z. Fang, G. F. Chen, J. L. Luo, and N. L. Wang, Observation of Fermi-surface-dependent nodeless superconducting gaps in $Ba_{0.6}K_{0.4}Fe_2As_2$, *Europhys. Lett.* **83**, 47001 (2008).
- [25] K. Terashima, Y. Sekiba, J. H. Bowen, K. Nakayama, T. Kawahara, T. Sato, P. Richard, Y.-M. Xu, L. J. Li, G. H. Cao, Z.-A. Xu, H. Ding, and T. Takahashi, Calorimetric study of single-crystal $CsFe_2As_2$, *Proc. Natl. Acad. Sci. USA* **106**, 7330 (2009).
- [26] X. G. Luo, M. A. Tanatar, J.-Ph. Reid, H. Shakeripour, N. Doiron-Leyraud, N. Ni, S. L. Bud'ko, P. C. Canfield, H. Q. Luo, Z. S. Wang, H.-H. Wen, R. Prozorov, and L. Taillefer, Quasiparticle heat transport in single-crystalline $Ba_{1-x}K_xFe_2As_2$: Evidence for a k-dependent superconducting gap without nodes, *Phys. Rev. B* **80**, 140503(R) (2009).
- [27] F. Hardy, A. E. Böhmer, D. Aoki, P. Burger, T. Wolf, P. Schweiss, R. Heid, P. Adelman, Y. X. Yao, G. Kotliar, J. Schmalian, and C. Meingast, Evidence of Strong Correlations and Coherence-Incoherence Crossover in the Iron Pnictide Superconductor KFe_2As_2 , *Phys. Rev. Lett.* **111**, 027002 (2013).
- [28] P. Werner, M. Casula, T. Miyake, F. Aryasetiawan, A. J. Millis, and S. Biermann, Satellites and large doping and temperature dependence of electronic properties in hole-doped $BaFe_2As_2$, *Nat. Phys.* **8**, 331 (2012).
- [29] Y. Liu and T. A. Lograsso, Crossover in the magnetic response of single-crystalline $Ba_{1-x}K_xFe_2As_2$ and Lifshitz critical point evidenced by Hall effect measurements, *Phys. Rev. B* **90**, 224508 (2014).
- [30] P. Popovich, A. V. Boris, O. V. Dolgov, A. A. Golubov, D. L. Sun, C. T. Lin, R. K. Kremer, and B. Keimer, Specific Heat Measurements of $Ba_{0.68}K_{0.32}Fe_2As_2$ Single Crystals: Evidence for a Multiband Strong-Coupling Superconducting State, *Phys. Rev. Lett.* **105**, 027003 (2010).
- [31] G. Mu, H. Luo, Z. Wang, L. Shan, C. Ren, and H. H. Wen, Low temperature specific heat of the hole-doped $Ba_{0.6}K_{0.4}Fe_2As_2$ single crystals, *Phys. Rev. B* **79**, 174501 (2009).
- [32] T. Terashima, M. Kimata, N. Kurita, H. Satsukawa, A. Harada, K. Hazama, M. Imai, A. Sato, K. Kihou, C.-H. Lee, H. Kito, H. Eisaki, A. Iyo, T. Saito, H. Fukazawa, Y. Kohori, H. Harima, and S. Uji, Fermi Surface and Mass Enhancement in KFe_2As_2 from de Haas-van Alphen Effect Measurements, *J. Phys. Soc. Jpn.* **79**, 053702 (2010).
- [33] S. Backes, D. Guterding, H. O. Jeschke, and R. Valentí, Electronic structure and de Haas-van Alphen frequencies in KFe_2As_2 within LDA+DMFT, *New J. Phys.* **16**, 083025 (2014).
- [34] S. L. Skornyakov, V. I. Anisimov, and D. Vollhardt, Effect of correlations and doping on the spin susceptibility of iron pnictides: The case of KFe_2As_2 , *JETP Lett.* **100**, 120 (2014).
- [35] J. G. Storey, J. W. Loram, J. R. Cooper, Z. Bukowski, and J. Karpinski, Electronic specific heat of $Ba_{1-x}K_xFe_2As_2$ from 2 to 380 K, *Phys. Rev. B* **88**, 144502 (2013).
- [36] A. E. Böhmer, Ph.D. thesis, Karlsruhe, 2014.
- [37] Z. Shermadini, J. Kanter, C. Baines, M. Bendele, Z. Bukowski, R. Khasanov, H.-H. Klauss, H. Luetkens, H. Maeter, G. Pascua, B. Batlogg, and A. Amato, Microscopic study of the superconducting state of the iron pnictide $RbFe_2As_2$ via muon spin rotation, *Phys. Rev. B* **82**, 144527 (2010).
- [38] V. I. Anisimov, A. I. Poteryaev, M. A. Korotin, A. O. Anokhin, and G. Kotliar, First-principles calculations of the electronic structure and spectra of strongly correlated systems: Dynamical mean-field theory, *J. Phys.: Condens. Matter* **9**, 7359 (1997).
- [39] K. Held, I. A. Nekrasov, G. Keller, V. Eyert, N. Blümer, A. K. McMahan, R. T. Scalettar, T. Pruschke, V. I. Anisimov, and D. Vollhardt, Realistic investigations of correlated electron systems with LDA + DMFT, *Phys. Stat. Sol. B* **243**, 2599 (2006).
- [40] G. Kotliar, S. Y. Savrasov, K. Haule, V. S. Oudovenko, O. Parcollet, and C. A. Marianetti, Electronic structure calculations with dynamical mean-field theory, *Rev. Mod. Phys.* **78**, 865 (2006).
- [41] F. Lechermann, A. Georges, A. Poteryaev, S. Biermann, M. Posternak, A. Yamasaki, and O. K. Andersen, Dynamical mean-field theory using Wannier functions: A flexible route to electronic structure calculations of strongly correlated materials, *Phys. Rev. B* **74**, 125120 (2006).
- [42] D. Guterding, S. Backes, H. O. Jeschke, and R. Valentí, Origin of the superconducting state in the collapsed tetragonal phase of KFe_2As_2 , *Phys. Rev. B* **91**, 140503(R) (2015).
- [43] J. Diehl, S. Backes, D. Guterding, H. O. Jeschke, and R. Valentí, Correlation effects in the tetragonal and collapsed-tetragonal phase of $CaFe_2As_2$, *Phys. Rev. B* **90**, 085110 (2014).
- [44] S. Mandal, R. E. Cohen, and K. Haule, Pressure suppression of electron correlation in the collapsed tetragonal phase of

- CaFe₂As₂: A DFT-DMFT investigation, *Phys. Rev. B* **90**, 060501(R) (2014).
- [45] F. Eilers, K. Grube, D. A. Zocco, T. Wolf, M. Merz, P. Schweiss, R. Heid, R. Eder, R. Yu, J.-X. Zhu, Q. Si, T. Shibauchi, and H. v. Löhneysen, Quantum criticality in AFe₂As₂ with A = K, Rb, and Cs suppresses superconductivity, [arXiv:1510.01857](https://arxiv.org/abs/1510.01857).
- [46] Hung T. Dang, Jernej Mravlje, Antoine Georges, and Andrew J. Millis, Electronic correlations, magnetism, and Hund's rule coupling in the ruthenium perovskites SrRuO₃ and CaRuO₃, *Phys. Rev. B* **91**, 195149 (2015).
- [47] S. Biermann, L. de' Medici, and A. Georges, Non-Fermi-Liquid Behavior and Double-Exchange Physics in Orbital-Selective Mott Systems, *Phys. Rev. Lett.* **95**, 206401 (2005).
- [48] Th. Pruschke and R. Bulla, Hund's coupling and the metal-insulator transition in the two-band Hubbard model, *Eur. Phys. J. B* **44**, 217 (2005)
- [49] A. E. Antipov, I. S. Krivenko, V. I. Anisimov, A. I. Lichtenstein, and A. N. Rubtsov, Role of rotational symmetry in the magnetism of a multiorbital model, *Phys. Rev. B* **86**, 155107 (2012)
- [50] P. Blaha, K. Schwarz, G. K. H. Madsen, D. Kvasnicka, and J. Luitz, WIEN2k, An Augmented Plane Wave Plus Local Orbitals Program for Calculating Crystal Properties (Karlheinz Schwarz, Techn. Universität Wien, Austria, 2001).
- [51] J. Ferber, K. Foyevtsova, H. O. Jeschke, and R. Valentí, Unveiling the microscopic nature of correlated organic conductors: The case of κ -(ET)₂Cu[N(CN)₂]Br_xCl_{1-x}, *Phys. Rev. B* **89**, 205106 (2014).
- [52] P. Werner, A. Comanac, L. de' Medici, M. Troyer and A. J. Millis, Continuous-Time Solver for Quantum Impurity Models, *Phys. Rev. Lett.* **97**, 076405 (2006).
- [53] B. Bauer, L. D. Carr, H. G. Evertz, A. Feiguin, J. Freire, S. Fuchs, L. Gamper, J. Gukelberger, E. Gull, S. Guertler *et al.*, The ALPS project release 2.0: open source software for strongly correlated systems, *J. Stat. Mech. Theory Exp.* (2011) P05001.
- [54] E. Gull, P. Werner, S. Fuchs, B. Surer, T. Pruschke, and M. Troyer, Continuous-time quantum Monte Carlo impurity solvers, *Comput. Phys. Commun.* **182**, 1078 (2011).
- [55] K. Haule, T. Birol, and G. Kotliar, Covalency in transition-metal oxides within all-electron dynamical mean-field theory, *Phys. Rev. B* **90**, 075136 (2014).
- [56] K. Haule, Exact double-counting in combining the Dynamical Mean Field Theory and the Density Functional Theory, *Phys. Rev. Lett.* **115**, 196403 (2015).
- [57] V. I. Anisimov, I. V. Solovyev, M. A. Korotin, M. T. Czyzyk, and G. A. Sawatzky, Density functional theory and NiO photoemission spectra, *Phys. Rev. B* **48**, 16929 (1993).
- [58] S. L. Dudarev, G. A. Botton, S. Y. Savrasov, C. J. Humphreys, and A. P. Sutton, Electron-energy-loss spectra and the structural stability of nickel oxide: An LSDA+U study, *Phys. Rev. B* **57**, 1505 (1998).
- [59] A. I. Liechtenstein, V. I. Anisimov, and J. Zaanen, Density-functional theory and strong interactions: Orbital ordering in Mott-Hubbard insulators, *Phys. Rev. B* **52**, R5467(R) (1995).
- [60] K. S. D. Beach, Identifying the maximum entropy method as a special limit of stochastic analytic continuation, [arXiv:cond-mat/0403055](https://arxiv.org/abs/cond-mat/0403055).
- [61] H. Eschrig and K. Koepnick, Tight-binding models for the iron-based superconductors, *Phys. Rev. B* **80**, 104503 (2009).
- [62] K. Koepnick and H. Eschrig, Full-potential nonorthogonal local-orbital minimum-basis band-structure scheme, *Phys. Rev. B* **59**, 1743 (1999); <http://www.FPLO.de>.
- [63] M. J. Calderón, B. Valenzuela, and E. Bascones, Tight-binding model for iron pnictides, *Phys. Rev. B* **80**, 094531 (2009)